

The SAGE Photometric Sky Survey: Technical Description

Zheng Jie^{1,2}, Zhao Gang^{1,2}, Wang Wei^{1,3}, Fan Zhou¹, Tan Ke-Feng¹, Li Chun¹ and Zuo Fang¹

¹ Key Laboratory of Optical Astronomy, National Astronomical Observatories, Chinese Academy of Sciences, Beijing 100101, China; gzhao@nao.cas.cn

² School of Astronomy and Space Science, University of Chinese Academy of Sciences, Beijing 100049, China

³ Chinese Academy of Sciences South America Center for Astronomy, China-Chile Joint Center for Astronomy, National Astronomical Observatories, Chinese Academy of Sciences, Beijing 100101, China

Abstract To investigate in more details of Stellar Abundance and Galactic Evolution (SAGE) and in a huge sample, we are performing a northern sky photometric survey named SAGES with the SAGE photometric system, which consists of 8 filters: Strömgren-*u*, SAGE-*v*, SDSS *g*, *r*, *i*, DDO-51, $H\alpha_{wide}$, and $H\alpha_{narrow}$, including three Sloan broadband filters, three intermediate-band filters and two narrow-band filters, and one newly-designed narrow-band filter. SAGES covers $\sim 12,000$ square degrees of the northern sky with $\delta > -5^\circ$, excluding the Galactic disk ($|b| < 10^\circ$) and the sky area of $12 \text{ hr} < \text{R.A.} < 18 \text{ hr}$. The photometric detection limit depth at signal-to-noise ratio 5σ can be as deep as $V \sim 20$ mag. The SAGES will produce a depth-uniformed photometric catalogue for ~ 500 million stars with atmospheric parameters including effective temperature T_{eff} , surface gravity $\log g$, and metallicity $[\text{Fe}/\text{H}]$, as well as interstellar extinction to each individual target. In this work, we will briefly introduce the SAGE photometric system, the SAGE survey, and a preliminary test field of the open cluster NGC 6791 and around.

Key words: methods: observational — techniques: photometric — surveys — astrometry — catalogues

1 INTRODUCTION

Astronomy is a basic science highly relying on the development of observations, and sky surveys on large areas are the most important ladders for the progress of astronomy. In recent decades, SDSS (York et al. 2000), 2MASS (Skrutskie et al. 2006) and other sky surveys have proved that mass data are very important, which lead to numerous new objects, new events, and new physics, and some even open

example LAMOST (Zhao et al. 2012) provides the most massive spectrum in the world, and plays an important role in finding metal-poor stars (Li et al. 2015), high- or hyper-velocity stars (Li et al. 2015), white dwarfs (Zhao et al. 2013), emission line objects (Shi et al. 2014).

As far as we know, the Geneva-Copenhagen Survey (GCS, Nordström et al. 2004) is the only sky survey on the Strömgren-Crawford (SC) system (Strömgren 1963, Strömgren 1964, Crawford et al. 1970), which includes intermediate and narrow band filters, dedicated to stellar atmospheric parameters. The GCS survey is volume complete to a distance of 40 pc down to $V \sim 8.5$ mag. The HM catalogue (Hauck & Mermilliod 1998) collected all measurements in these systems, which include only $\sim 66,000$ stars in total. This situation is mainly due to the fact that it requires much more integration time in the narrow and medium-band, especially in the Strömgren- u and $H\beta_n$ -bands, than broadband filters, to achieve similar brightness limit. With the development of CCD photometry, a much better sensitivity in the blue of CCD detectors, and the emergence of tens of 4-10m telescopes, it is now a best opportunity to conduct a sky survey with a number of small infrequently-used smaller aperture telescopes with wide-field cameras in narrow and medium bandpasses which is dedicated to the determinations of atmospheric parameter of stars much fainter than GCS.

However, among all the previous or currently ongoing sky surveys, few of them are specifically focused on stellar atmospheric parameters. Under this situation, we are performing a deep photometric sky survey using a combination of narrow, intermediate and broadband filters, with the main purpose to determine stellar parameters for hundreds of millions of stars with accuracies significantly better than those obtained with broadband filters and comparable to those determined spectroscopically. We will introduce the design of our sky survey and observations, and the data reduction pipeline, and our performance test field as a sample.

2 THE SAGE PHOTOMETRIC SKY SURVEY AND OBSERVATION

2.1 The SAGE Photometric System

The Johnson UBV photometric system (Johnson & Morgan 1953) is one of the earliest and most used among all standard photoelectric photometric systems. While the revolutionary project SDSS, by providing an unprecedented database of photometric observations of stars and galaxies, has essentially made its bandpasses, the SDSS photometric system, u'g'r'i'z' (Fukugita et al., 1996), the current standard for most (if not all) ongoing and future photometric surveys and most photometric imaging. However, it is unfortunate that SDSS filters were chosen basically to determine photometric redshifts for galaxies, rather than to isolate relevant stellar absorption features in particular bands, and therefore this system is not ideal for accurate determinations for the metallicities and gravity of stars.

Thanks to narrower bandpasses and specific definition in u band, the Strömgren-Crawford (SC) system provides a reliable method to determine stellar parameters for stars with a wide range of spectral types (e.g., early or late type stars, metal-poor stars). In particular, this photometric system, composed of the Strömgren $ubvy$ plus the $H\beta$ wide and narrow bandpasses, can accurately identify stars at various evolutionary stages

$v)-(v-b)$, $\beta = \beta_n - \beta_w$ could be used to measure metallicity and surface gravity, and the strength of H β line without being affected by extinction.

In order to obtain accurate stellar atmosphere parameters with high efficiency, we constructed a new photometric system: the SAGE system, by combining multiple photometric systems, and adding several new filters. This system consists of 8 filters: Strömgren- u , SAGE- v , SDSS g , r , i , DDO-51, $H\alpha_{wide}$, and $H\alpha_{narrow}$ (hereafter u_{SC} , v_{SAGE} , g , r , i , DDO51, $H\alpha_w$ and $H\alpha_n$, respectively). The effective wavelengths and bandwidths of them are shown in Table 1 and their normalized transmission curves are plotted in Fig. 1. All magnitudes of the SAGE system are on the AB system.

The SAGE system can effectively determine stellar atmospheric parameters, including effective temperature T_{eff} , surface gravity $\log g$, and metallicity [Fe/H], as well as extinction. These parameters can be determined by $(g-i)$, $(u_{SC}-v_{SAGE})$, $(v_{SAGE}-g)$, and $(H\alpha_n - H\alpha_w)$ in the system. The response curves of the u_{SC} and v_{SAGE} filters are located on both sides of the Balmer jump and can be used to measure its intensities. Moreover, there is almost no overlapping area between the two filters of the SAGE system, and more accurate $\log g$ measurement results can be obtained. We prefer our v_{SAGE} than Strömgren- v as it is bluer by $\sim 150\text{\AA}$, aiming to include Ca II H & K doublets for better correlation with stellar metallicities. The SDSS g and r filters should have similar usages as Strömgren b and y , while they will consume significantly less amount of observation time with the latter two. We change the H β filters to H α ones as the CCD efficiency is similar at both wavelengths, while the latter ones have stronger imprints on stellar or nebular spectra, and therefore should have higher sensitivity. In G- and K-type stars, H β lines are weaker than H α ones, so measurement on these lines will be more efficient. The DDO51 filter is employed to further constrain stellar gravity. For more details, please refer to Fan et al. (2018).

Table 1: The SAGE Photometric System

Band	u_{SC}	v_{SAGE}	g	r	i	DDO51	$H\alpha_n$	$H\alpha_w$
Effective wavelength (\AA)	3520	3950	4639	6122	7439	5132	6563	6563
Bandwidth (\AA)	314	290	1280	1150	1230	162	29	136

2.2 The SAGE Photometric Sky Survey

The SAGE Photometric Sky Survey (SAGES) is a northern sky survey with the SAGE photometric system on about 12,000 square degrees. This survey was firstly proposed in 2014 (Wang et al. 2014) to be conducted with the full set of the Strömgren-Crawford (SC) system. After further investigations, we believe our SAGE system is superior to the SC system, and the SAGE system is therefore adopted in our survey instead of the SC system. Since 2015, the SAGES has been started, and the plan is to finish observations, flux calibrations and astrometric calibrations in 4 to 5 years. We aim to achieve a survey depth at signal-to-noise ratio (SNR) 5:1 to 20 mag in the Johnson V band on Vega system, which corresponds to depths of ~ 21.5 in u_{SC} , ~ 21.0 in v_{SAGE} , and ~ 19.5 in g , r and i . Note that these are magnitudes on the AB system, and all flux and errors are measured from point sources extracted by Source Extractor (Bertin & Armouts 1996)

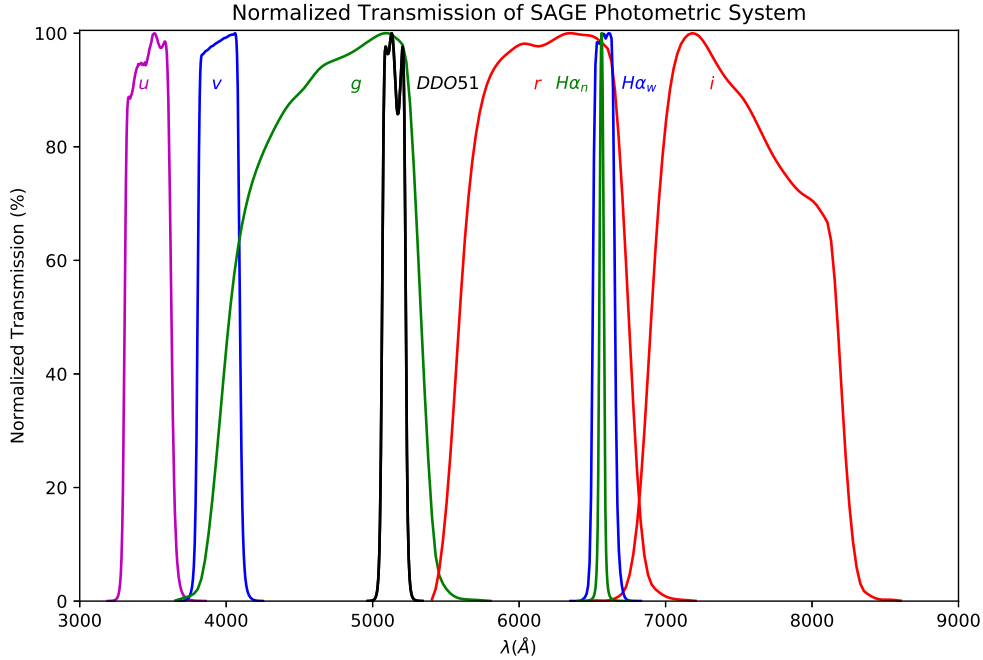


Fig. 1: The Normalized Transmission Curves of the SAGE Filters

The SAGES will produce a depth-uniformed photometric catalogue for ~ 500 million stars with atmospheric parameters including effective temperature T_{eff} , surface gravity $\log g$, and metallicity $[\text{Fe}/\text{H}]$, as well as extinction to each individual target. Value-added information like stellar radius may be provided as well when combined with high precision parallax measurements by the Gaia Mission (Gaia Collaboration et al. 2018).

To finish a whole northern sky survey with non-broad band filters takes a lot of telescope time even with wide-field cameras. Therefore, we decide to use three telescopes almost simultaneously to conduct the survey in different bandpasses, as described below. We note that with careful design of standard star observations, the absolute flux calibration is expected to be as good as 0.02 mag, and the uniformity to be better than 0.02 mag in our first data release, and shall be improved in later data releases.

2.3 Telescopes and Instruments

Given that the u_{SC} -band has a wavelength coverage very close to the atmospheric cutoff, plus the fact in this band typical stars are intrinsically very faint, therefore integration time in u_{SC} to achieve our proposed 5σ -limit of 21.5 mag. Considering to keep the observations in three different telescopes at the same pace, and the fact the Bok 90-inch telescope¹ has twice larger aperture than the other two, we decide to conduct the observations in u_{SC} and v_{SAGE} . The Bok telescope is an equatorial mounting telescope located at Kitt Peak, which is at $30^{\circ}57'46''.5\text{N}$ by $111^{\circ}36'01''.6\text{W}$, and 2071 meters above sea level. The Bok Telescope belongs to Steward Observatory, the University of Arizona.

The instrument named 90Prime consists of four $4\text{K} \times 4\text{K}$ back-illumination CCDs and is installed at the prime focus of the telescope. The field of view is around $1^{\circ}.08 \times 1^{\circ}.03$ with gaps of $\sim 166''$ at R.A.

and $\sim 54''$ at Decl between CCDs. Fig. 2 shows the layout of 90Prime. We choose the slow mode to read the whole frame of 90Prime, which takes about 37 seconds with a noise level of 6-10 electrons per pixel. We perform u_{SC} - and v_{SAGE} -band observations using the Bok telescope.

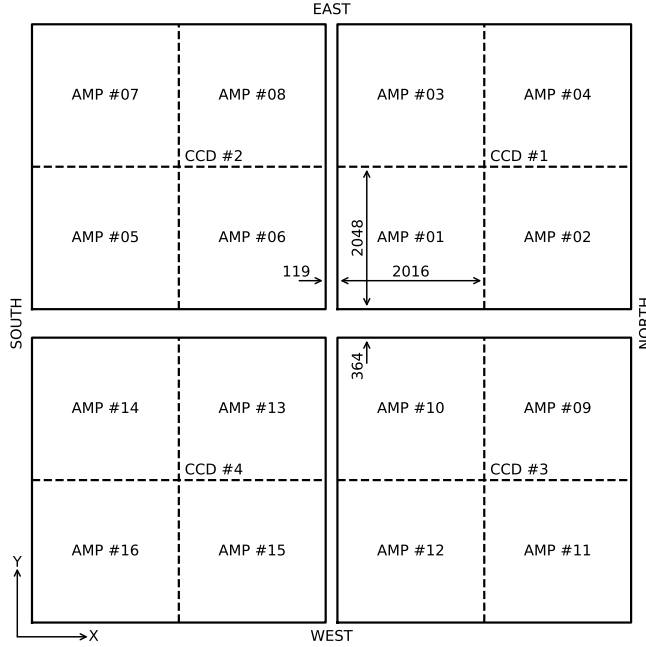


Fig. 2: The layout of 90Prime detector array. (Not to Scale, Pixel)

For the SDSS g , r and i -bands, we decide to use Nanshan One-meter Wide-field Telescope (hereafter, NOWT) to carry out observations. NOWT is an altazimuth-mounted telescope located at Nanshan Station, which is at $43^{\circ}16'45''.0\text{N}$ by $87^{\circ}10'38''.3\text{E}$, and 2081 meters above sea level. NOWT belongs to Xinjiang Astronomical Observatory (XAO), Chinese Academic of Sciences (CAS). A wide field camera, consisting of a $4\text{K}\times 4\text{K}$ blue-enhanced back-illumination CCD, is installed at the prime focus of NOWT, with a field of view of about $1^{\circ}.5 \times 1^{\circ}.5$. The typical readout speed is about 40 seconds via 4 parallel amplifiers with a readout noise of 8-10 electrons (Liu et al. 2014). As SDSS survey has covered $\sim 9,000$ square degrees in the northern sky, we only need to conduct the observations in gri -bands for the rest $\sim 4,000$ square degrees including some overlapping regions to secure flux calibrations.

The Zeiss-1000 Telescope at the Maidanak Astronomical Observatory, Ulugh Beg Astronomical Institute, Uzbek Academy of Sciences (MAO, Ehgamberdiev et al. 2000) is being upgraded, it is expected to be available in late 2018. Its current field of view is $32.9' \times 32.9'$. We will perform $H\alpha_w$ and $H\alpha_n$

2.4 Observations and progress

The SAGES is proposed to cover the northern sky with $\delta > -5^\circ$, excluding the bright, high extinction Galactic disk ($|b| < 10^\circ$). Meanwhile, because of the time allocation of Bok, we exclude the sky area of $12 \text{ hr} < \text{R.A.} < 18 \text{ hr}$ for the current observation, and may accomplish it in future projects. Fig. 3 demonstrates the proposed coverage of the SAGES.

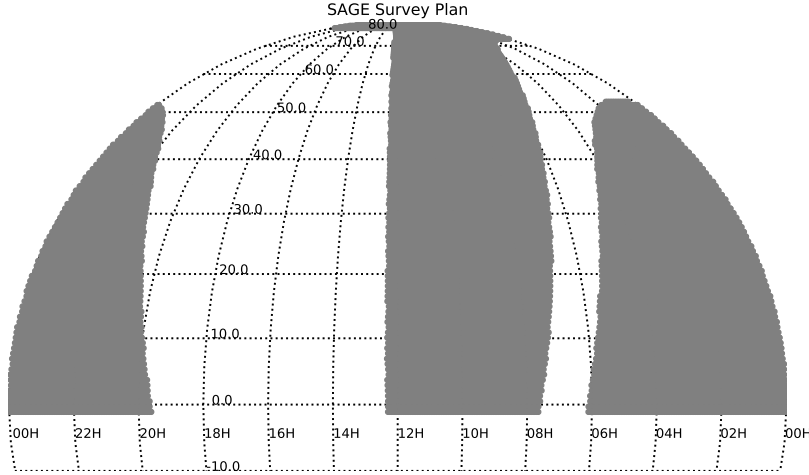


Fig. 3: Coverage Plan of the SAGE photometric Sky Survey

For all the observations at the three telescopes, we have the same strategy with the only differences are filters and exposure times. In clear nights, the exposure time for each band is listed in Table 2. The exposure times will increase as the airmass increases. They will also increase with the cloud. For each night we make a plan based on the previous footprint, and the current date, so that most fields are observed at lowest possible airmass, and the time for telescopes to slew is the shortest. Normally, a field will be observed only once for each band.

Table 2: Exposure time of each band in clear nights

Band	u_{SC}	v_{SAGE}	g	r	i
Exposure time (second)	60	20	30	40	40

To achieve reliable and consistent flux and astrometric calibrations, we leave sufficient overlapping regions between adjacent fields. The observation fields at the same Declination form a horizontal stripe, and in the stripe $\sim 20\%$ overlapping is reserved between adjacent fields in the same stripe. Meanwhile $\sim 20\%$ overlapping is set between adjacent stripes. As a result, each field will have one neighbour in the east and one in the west with $\sim 20\%$ overlapping region in each direction, and it has two northern and two southern neighbours with overlapping fractions of 0-20% for each field-to-field pair, but in total 20% for each direction. Fig. 4 shows the overlapping between Bok Field 6352 and its neighbours as an example, and the distributions are very similar with different field scales due to different size fields-of-view for the other

We estimate that $\sim 36\%$ of the survey area will be visited only once, and 32 – 48% of survey area will be visited twice, and $\sim 24\%$ to be visited three times, and the rest small fraction $< 16\%$ to be visited four times. The time span between visit could range from minute to days and to years. With multiple visits of in total 36% of our survey area, on one hand, reliable flux and astrometric calibrations could in principle achieved, and on the other hand, a time-domain alert should be able to be spotted out for future follow-up studies.

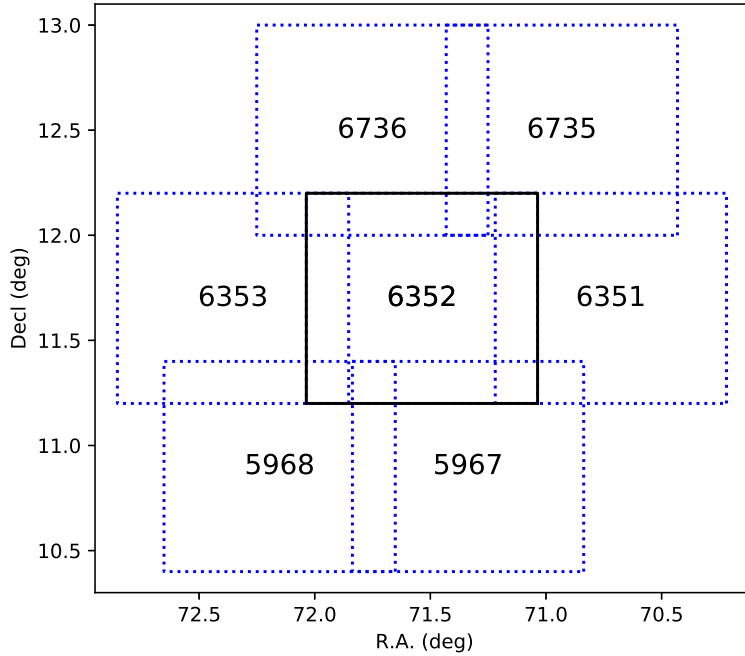


Fig. 4: Overlap between Survey Fields

The SAGES launches its observations in the autumn of 2015. By the end of Jan 2018, observations of g , r and i at NOWT are completed, meanwhile, observation of u_{SC} and v_{SAGE} on Bok are about 2/3 completed, and the rest 1/3 is expected to be done in 2019. Observations to be done at MAO is scheduled in late 2018. The current progress of the Survey as of January 2018 are listed in Table 3, and the up-to-date progress can be found at the official website of the SAGES².

Table 3: The observation progress of the SAGES as of January 2018.

Band	u_{SC}	v_{SAGE}	g	r	i
Field number	12364	11376	4254	4254	4254
Area covered (deg ²)	7913	7280	4254	4254	4254
Percent (%)	69.7	64.2	100.0	100.0	100.0

3 THE DATA REDUCTION PIPELINE

We have developed a data reduction pipeline, to semi-automatically perform standard reduction procedures including bias subtraction, flat-fielding, distortion correction, astrometry, and aperture photometry. We will introduce our pipeline briefly in this section, as shown in Fig. 5.

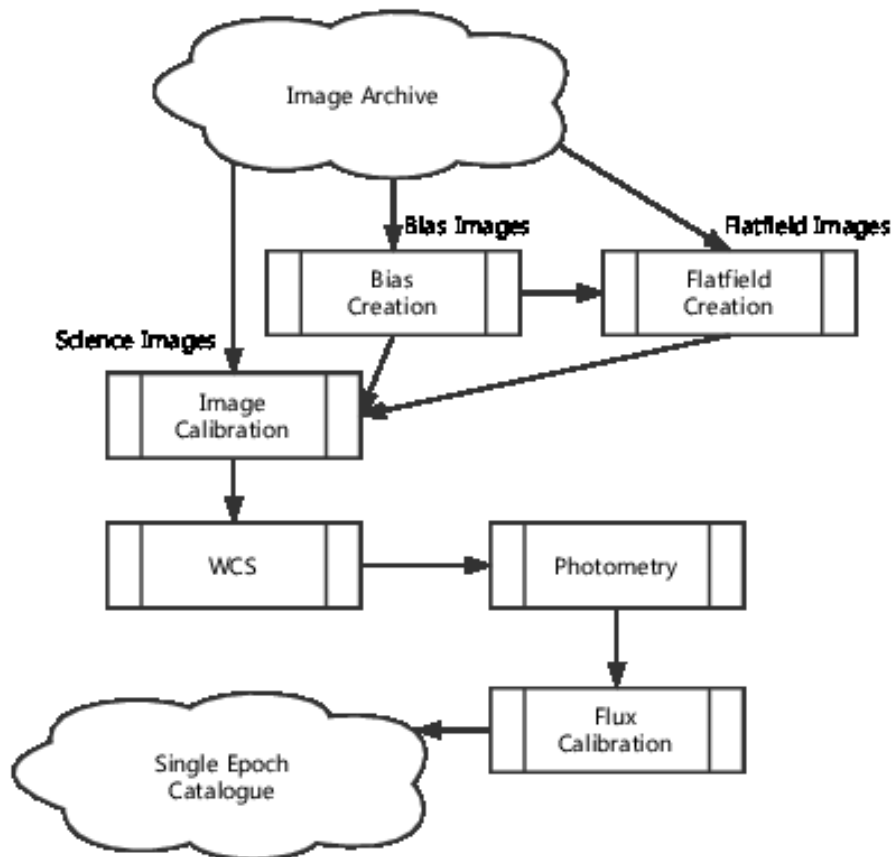


Fig. 5: The Flowchart of the Science Data Pipeline

3.1 Correction of Images

The ultimate purpose of image reduction is to convert detector digital counts given in raw CCD images to electron count rates (e^-/s), through a series of procedures including overscan and bias correction, flat-fielding, and crosstalk removing.

The pipeline computes the median value of each row of the overscan area, then subtracts it from the corresponding rows of the image. Following the technique performed in Zou et al. (2017) for the BASS data, which was obtained also with 90Prime, a Gaussian smoothing is applied to the counts variations in the row direction, which is believed to better represent bias level along the row direction. A section of the

science images, the overscan correction is the first step in data reduction. We use the same method to correct overscan at both Bok and NOWT after tests.

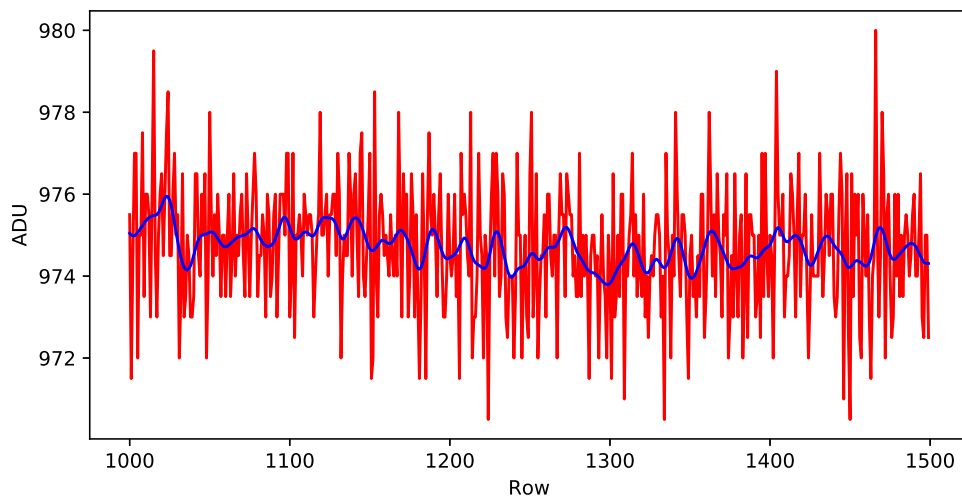


Fig. 6: ADU of overscan region (red) and a smoothed curve (blue)

Before and after each night of observations, a set of 10 bias exposures are taken. A master bias frame can be easily constructed, with each pixel's value to be the median value of the 20 exposures at the same pixels. With this master bias image, all science exposures and flat-field exposures taken on the same night can be bias-subtracted accordingly.

The next step is to perform flat-fielding for science exposures with flat-field exposures taken at the sky during twilight, or those taken on a curtain illuminated uniformly by a scanning lamp during the daytime, or super night-sky flat by merging all the science images taken over the night. As usual, the priority is to use high signal-to-noise ratio (SNR) twilight flats to correct large-scale illumination trend and employ the dome flats to correct for pixel-to-pixel variations when applicable, and if not, a super night-sky flat will be used instead. We estimate that our master flat images will be accurate to 1 percent for most nights.

The 90Prime consists of 4 CCDs, each has 4 amplifiers for parallel readout. This function of multi-channel CCD read-out can significantly reduce the time spent on reading the detector. The disadvantage of this option is the so-called amplifier cross-talk, which causes contamination across the output amplifiers, typically at the level of 1:10,000. It can be a serious problem for high precision photometry, and when bright stars saturate in CCD detectors.

We follow the method suggested by Freyhammer et al. (2001) to remove crosstalks. We compute the crosstalk coefficient from bright sources detected and their crosstalk signal on other amplifiers of the image. We use a large number of images to estimate the crosstalk coefficients between amplifiers. The pipeline computes the crosstalk pollution from bright areas with the coefficients, then apply it to correct the image. The overall ratio of crosstalk is about 5:10,000 for 90prime, while inter-CCD crosstalk ratios are greater and intra-CCD ratios are lower. Fig. 7 shows a typical crosstalk and the image after correction.

a-b are polluted by inter-CCD crosstalk. Panel g-k are corrected images of a-e, respectively. In panel j, the saturated area is marked. In all panels, the polluted and corrected areas are pointed out.

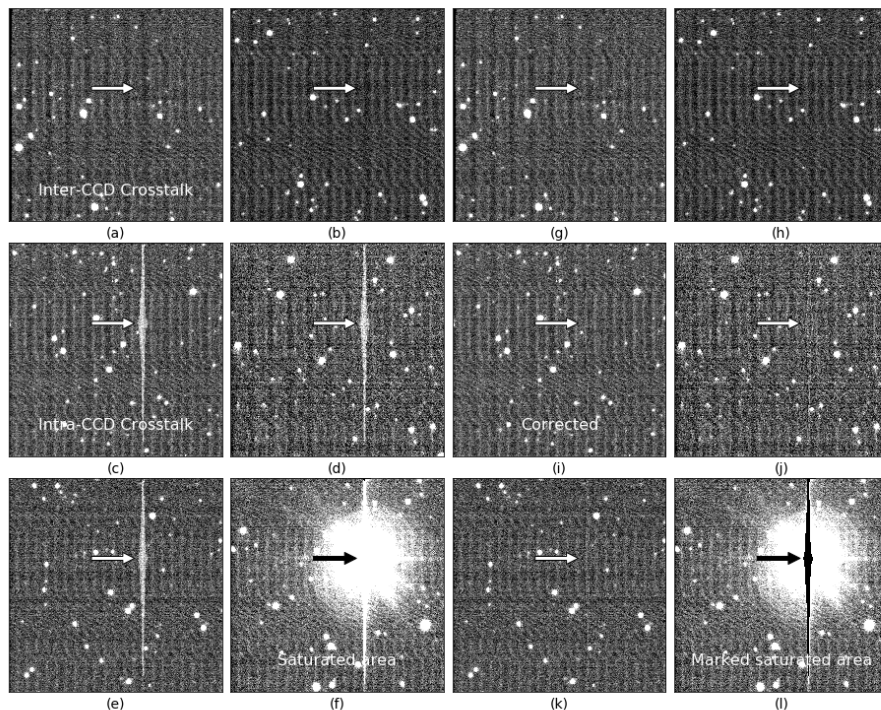


Fig. 7: A typical crosstalk and the image after correction in inverted gray scale. Panel a-f are original images. Panel f is the source, panel c-e are polluted by intra-CCD crosstalk, and panel a-b are polluted by inter-CCD crosstalk. Panel g-k are corrected images of a-e, respectively. In panel j, the saturated area is marked. In all panels, the polluted and corrected areas are pointed out. Stripes caused by interference from the camera controllers as large-scale patterns can be seen in images. We are working on this and they will be removed in the future.

In Fig. 7, stripes caused by interference from the camera controllers can be seen. They are large-scale patterns but not uniform and do not full-fill the whole image. We are working on this issue and they will be removed in the future version of the pipeline.

3.2 Astrometric Calibration

The astrometric calibration is realized in two steps. Firstly, the pipeline will work out a linear solution assuming the image has no distortion, based on the information stored in image headers, including the telescope pointing coordinates, the rotation angle, and the pixel scale.

For further corrections, the pipeline employees the package named Software for Calibrating AstroMetry

(Bertin & Armouts 1996) by matching SExtractor’s output catalogue with an online or local reference catalogue. SCAMP is mature and robust software that is widely used in astrometric calibration. The pipeline calls twice SCAMP. For the first one, a loose criterion for cross-matching detected sources with reference sources is used to retain enough stars for calibration. For the second run of SCAMP, a strict criterion is used to obtain precise solution based on previous results. Table 4 shows the major configuration parameters for SCAMP in the two calls. The configurations are same for both Bok and NOWT, especially we find `DISTORT_DEGREES = 3` is the most suitable configuration after a series of tests.

Table 4: The major configuration parameters for SCAMP.

Keyword	Round 1	Round 2	Note
<code>MATCH</code>	Y	Y	Module match or not
<code>MATCH_NMAX</code>	0	0	Up bound of cross match
<code>PIXSCALE_MAXERR</code>	2	1.5	Max error of pixel scale
<code>POSANGLE_MAXERR</code>	5.0	2.0	Max error of position angle (degrees)
<code>POSITION_MAXERR</code>	10.0	1.0	max error of position (arcminutes)
<code>MATCH_RESOL</code>	0	0	Matching resolving
<code>MATCH_FLIPPED</code>	N	N	Allow axis flipping in match or not
<code>CROSSID_RADIUS</code>	25.0	2.0	Cross identification radius (arcseconds)
<code>SOLVE_ASTROM</code>	Y	Y	Solve astrometric solution or not
<code>PROJECTION_TYPE</code>	<code>SAME</code>	<code>SAME</code>	Projection type
<code>DISTORT_DEGREES</code>	3	3	Degrees of distortion polynomial

The Position and Proper Motion Extended (PPMX, Roser et al. 2008) catalogue is adopted in our pipeline as the astrometric reference. PPMX contains about 18 million stars which are evenly distributed across the whole sky with accuracies of $\sim 0.02''$ in both R.A. and Decl. directions. Over 85% PPMX stars have V magnitudes between 10.0 and 15.0 mag, which matches very well with the dynamic ranges of our SAGES survey. As the Gaia DR2 (Gaia Collaboration et al. 2018) has just been released, we will use it as the astrometric reference in the future.

SDSS and Pan-STARRS DR1 (PS1, Chambers et al. 2016) are both accurate in astrometric and flux calibrations. But SDSS covers only part of all sky, so we cannot use it as the reference catalogue to ensure the uniformity of the correction. PS1 has an uncertainty lower than $0.005''$ in both R.A. and Decl, but it does not provide proper motions, so we do not use it as the astrometric reference, but we use it as the flux reference in Section 3.4.

Besides calling SCAMP, another astrometric calibration method is developed to provide an astrometric solution. Both methods are used in the pipeline so that we can compare their results to make sure we have the correct solution.

Generally, the purpose of the astrometric calibration is to fit a transforming formula from image coordinates (x, y) to celestial sphere coordinates (α, δ) , and then apply the formula to obtain the coordinates of all detected objects. The transforming formula is usually linear functions if there are not significant image

and the field-of-views are both larger than 1 deg^2 , the image distortions cannot be ignored and should be corrected.

The first step is to convert the original pixel coordinates (x, y) with origin at the left-bottom corner, to intermediate pixel coordinates (u, v) with the origin at the center of the image. Then (u, v) is converted to intermediate world coordinates (ξ, η) using parameters CDi_j in the image header. Finally, (ξ, η) is projected to the world coordinates (α, δ) , depending on the projection type, and our pipeline adopts the type ‘TAN’. To resolve non-linear correlation between (ξ, η) and (α, δ) , we use SIP (Simple Imaging Polynomial, Shupe et al. 2005) convention to represent image distortion. SIP adds high-order correcting polynomials f and g to u and v to express the distortion, as shown in formula 1.

$$\begin{pmatrix} \xi \\ \eta \end{pmatrix} = CD \times \begin{pmatrix} u + f(u, v) \\ v + g(u, v) \end{pmatrix} \quad (1)$$

To determine polynomials f and g , A_{pq} and B_{pq} are used as the coefficients of $u^p v^q$ as shown in Formula 2, in which N_A and N_B are the highest order to correct u and v , respectively. After comprehensive tests, we find $N_A = N_B = 3$ is appropriate for the SAGES.

$$\begin{aligned} f(u, v) &= \sum_{p,q} A_{pq} \cdot u^p v^q, & 2 \leq p + q \leq N_A \\ g(u, v) &= \sum_{p,q} B_{pq} \cdot u^p v^q, & 2 \leq p + q \leq N_B \end{aligned} \quad (2)$$

To evaluate internal astrometric errors yielded by the SAGES pipeline, comparisons have been made for all the fields with multiple visits, either in the same band, or in different bands, and calculate the differences in coordinates between different visits. Fig. 8 shows a typical internal astrometric error, in which we find that $\Delta R.A. = 0''.014 \pm 0''.145$ and $\Delta Decl = -0''.002 \pm 0''.166$.

We determine the external astrometric errors by computing the difference between the computed coordinates and matched coordinates from the reference catalogue PPMX. Fig. 9 shows a typical distribution of external astrometric calibration errors. The errors are reasonable, with marginal offsets and small standard deviations of $\sim 0.1''$ in both R.A. and Decl, as marked in the lower-left panel of Fig. 9. In conclusion, the internal and external astrometric uncertainties in SAGES are $\sim 0.1''$ in both directions. It can be improved in the future when employing Gaia DR2 as reference catalogue.

3.3 Source Detection and Aperture Photometry

To detect sources and perform photometric measurements, the software Source Extractor (SE, Bertin & Armouts 1996) is used in the SAGES pipeline. We set the detection threshold to be 4, which secure that most sources could be found and measured by SE. After a successful run, SE will determine for each source the following information with uncertainties: the central positions of each source in both CCD physical coordinates and celestial coordinates, the roundness and sharpness, instrument magnitudes included in given aperture size(s). It will produce photometric results using different methods, among which some are appropriate for point sources and others for extended sources. Following the exercises in other surveys like SDSS (York et al. 2000) and SkyMapper (Wolf et al. 2018), we use the SE output MAG_AUTO as our primary output, as this output is in general reliable for both point sources and extended sources. The

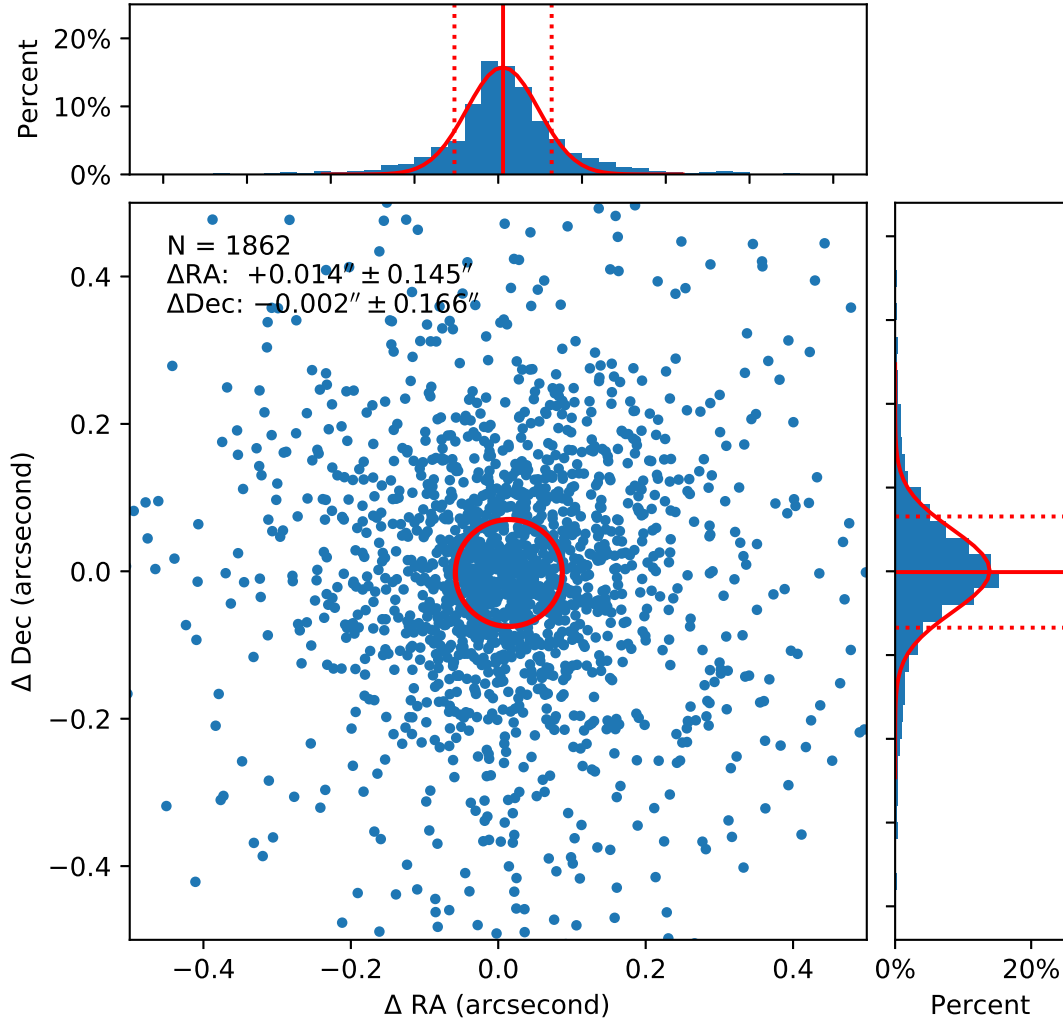


Fig. 8: Typical internal error of the astrometric results yielded by the SAGES pipeline, as compared to PPMX. The number of stars used for comparisons, the offsets, and standard deviations are marked in the lower-left panel. In top and right panel, the histograms of the differences in R.A. and Decl. are plotted, respectively, with best-fit Gaussian-profile overplotted in red.

Source detection and photometry are performed on a CCD basis, and a global aperture size is adopted for all the stars in one CCD. However, it is well known that a compromised aperture size, which is in general small, has the advantage to produce the smallest photometric errors for faint stars, however, aperture correction must be applied to them. We follow the process described in Howell (1989) to make accurate corrections using the aperture growth-curve method.

3.4 Flux Calibration

To achieve scientific goals of accurate determinations of stellar parameters, the SAGES is required to yield photometry of stars brighter than 15 mag in V with accuracies better than 0.01 mag. To meet this require-

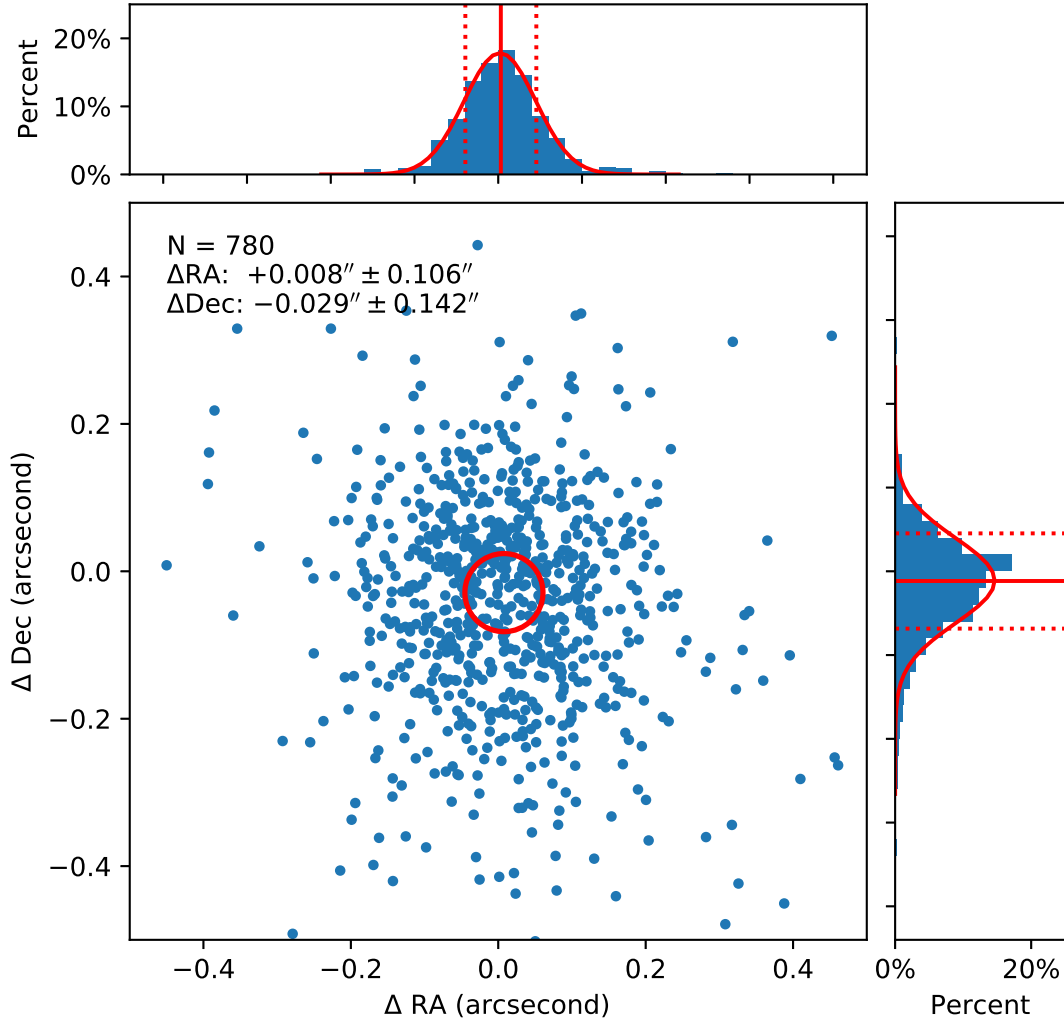


Fig. 9: The same as Fig. 8, but for typical external error.

Table 5: The major configuration parameters of for Source Extractor

Argument	Value	Note
DETECT_MINAREA	5	Minimum area of detection
DETECT_THRESH	4.0	Detection threshold
ANALYSIS_THRESH	4.0	Threshold of analysis
PHOT_AUTOPARAMS	2.5, 3.5	Parameters to measure MAG_AUTO , Kron factor and minimum diameter
SATUR_LEVEL	45000.0	Saturation level before normalization
MAG_ZEROPOINT	25.0	Zeropoint of instrumental magnitude

To correct for atmospheric extinction and transfer the instrument magnitude to apparent magnitude for the SAGES survey, we use two methods by using standard stars or existing photometric surveys with well-calibrated photometry. In a photometric night, multiple observations on a set of standard stars are conducted

to calibrate the apparent magnitude of stars observed in that night and any other photometric nights. In Fig. 10, we show the extinction curves derived in u_{SC} & v_{SAGE} on Sep. 23th and 24th, 2017 as examples.

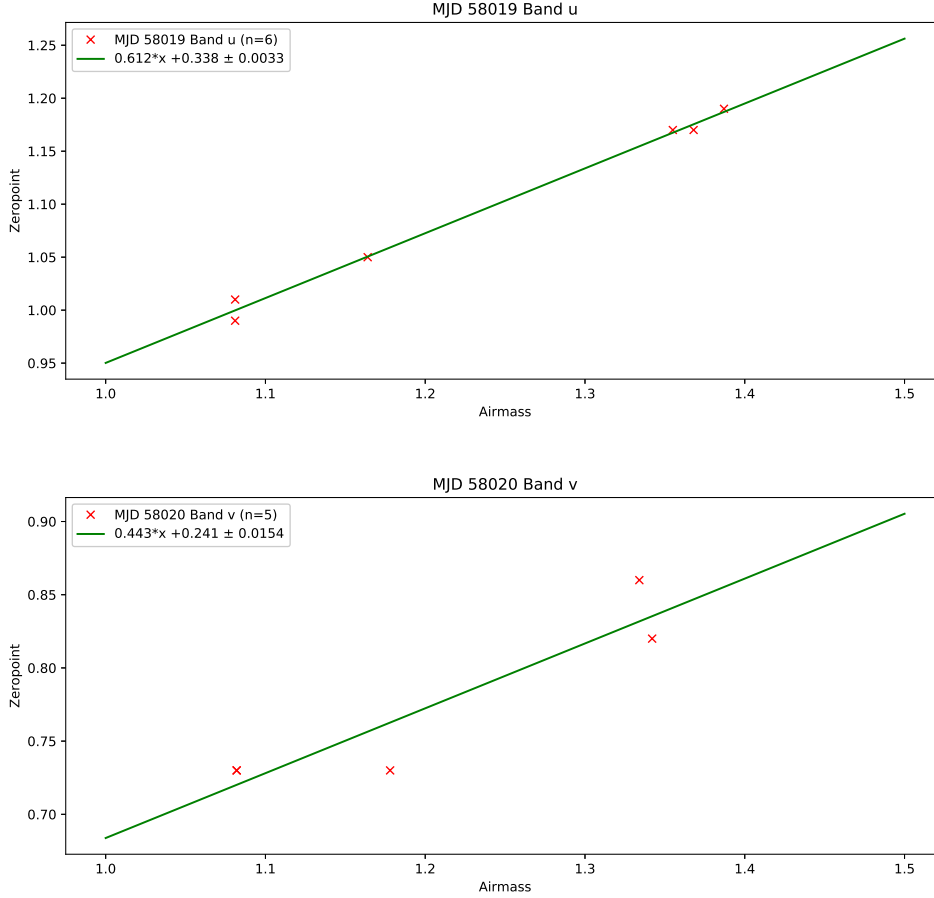


Fig. 10: The atmospheric extinction curves derived for u_{SC} & v_{SAGE} on Sep. 23 and 24th, respectively at Kitt Peak.

For non-photometric nights, we have to rely on real-frame flux calibration by using the stars with high-precision magnitudes provided by previous surveys or catalogues. For the SAGES, we use the Panoramic Survey Telescope and Rapid Response System Data Release 1 (Pan-STARRS DR1, Chambers et al. 2016) as the reference for flux calibration.

For the two filters u_{SC} and v_{SAGE} that have not been covered by Pan-STARRS DR1, we derived their magnitudes with a method trained from the g , r and i magnitudes. We select candidate stars from spectrum library by Pickles (1998). We convolve their spectrum with each filter transmission curve to determine photometry in each band, with which we fit polynomial correlations between u_{SC} and v_{SAGE} with g , r , and i as shown in Equation 3. With the derived correlation, and the reddening maps given by Schlegel et al. (1998), for each Pan-STARRS DR1 star, its apparent u_{SC} & v_{SAGE} magnitudes can be determined accordingly.

$$u_0 = i_0 + 0.441 + 2.721(g - i)_0 \quad (3)$$

The derived magnitudes can only be used to estimate the observation depth and the data quality. We are planning to perform calibrating observations in several photometric nights, in order to achieve a secondary flux reference catalogue which can be used to calibrate all observation fields in all kind of nights.

To evaluate the overall internal uncertainties of our image reduction, photometry, and flux calibration, we differ the calibrated photometry of the same stars in different observations against photometry in Fig. 11. The top and bottom panels are for the u_{SC} & v_{SAGE} bands, respectively. The x-axis is calibrated magnitudes, and the y-axis is the difference between two exposures. The red curves show the 3σ loci by binning of 1.0 mag. We can find from the figure that the depths at SNR 5 : 1 are $u_{SC} \sim 20$ mag and $v_{SAGE} \sim 19.5$ mag, and the depths at SNR 100 : 1 are $u_{SC} \sim 16.5$ mag and $v_{SAGE} \sim 15.5$ mag. The depths are almost satisfied with our aim. It is obvious that the internal photometric measurements need to be improved. We note that the $\sim 20\%$ overlapping regions between adjacent fields will be very helpful to secure high-accuracy internal consistency in the entire survey area, and therefore the final uncertainties of flux calibrations should be similar or just slightly larger than those obtained with photometric stars observed in photometric nights.

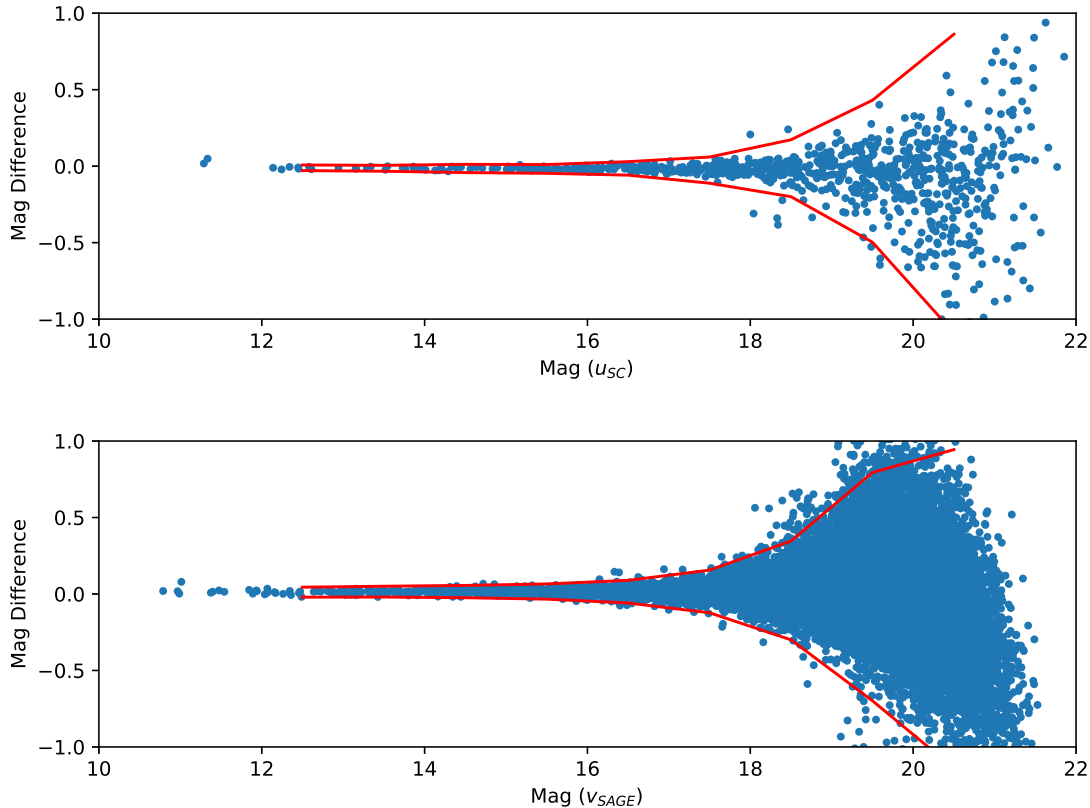


Fig. 11: The internal photometric uncertainties against photometry for u_{SC} (top) & v_{SAGE} (bottom). The red curves show the 3σ loci.

4 TESTING FIELD OF NGC 6791 AND ITS RESULT

4.1 Calibration Observations of NGC 6791

Wide-field imaging bears serious problems for accurate photometry, due to field distortions, imperfect image quality near the edges of the field-of-view of the camera, and the uniformity of detectors and amplifiers in a large format of the mosaic camera. It turns to be even difficult for narrow- and medium-band filters, as for the case of fast focal ratio, the transmission curve might change from the center to the edge of the field-of-view.

To fully understand the situation in the instrument that we are using, and to make reliable field corrections, we performed a set of test observations of NGC 6791 on Sep. 15th, 2017. NGC 6791 is a well studied open cluster, centered at 19:20:50.7 +37:45:38.4 with an approximate diameter as 0.2 degrees (Warren & Cole 2009, Smolinski et al. 2011, Basu et al. 2011, Mészáros et al. 2013, Tofflemire et al. 2014, Hawkins et al. 2016). The angular size of NGC 6791 fits well into one amplifier of the 90Prime camera at the Bok telescope, and therefore it is appropriate to study the relative offsets between the 16 amplifiers of the 90Prime camera.

For each of the u_{SC} and v_{SAGE} filters, 16 exposures were taken at slightly different sky positions with each pointing NGC 6791 locates at one of the 16 amplifiers. As a test, we used longer exposure times than regular survey observations, 100 s for u_{SC} and 40 s for v_{SAGE} . It was clear, and the median FWHM of point sources detected in all images was $\sim 1.7''$. The coverage of our test observations as the blue box is shown in Fig. 12, while the 16 small crosses are the center of each pointing, the $1.08^\circ \times 1.03^\circ$ green dotted box presents one example field pointing to the green cross. The red stars demonstrate the identified cluster members of NGC 6791 from works listed above.

4.2 Results of the Testing Field

We have reduced and analyzed the testing observation data, and have detected 109,472 objects in u_{SC} -band and 215,092 objects in v_{SAGE} -band with 4σ . The magnitude limits for single-exposure images are estimated by the APER magnitudes error at about 0.20 and 0.02 mag, which correspond to the SNR of 5 and 50, respectively. The median u_{SC} - and v_{SAGE} -band depths are 20.05 and 21.30 at 5σ and 17.16 and 18.37 at 50σ by the exposure times of 100 s and 40 s in u_{SC} and v_{SAGE} -band, respectively.

We plot the detected point sources in color-color diagrams in Fig. 13 as blue dots. For comparisons, synthetic colors of stars from the MILES stellar library (Falcón-Barroso et al. 2011) by convolving the transmission curves with the stellar spectrum, are overplotted in red. The measurements of g , r and i are taken from Pan-STARRS DR1. In the left panel, the bifurcation between cool dwarfs and cool giants is clear.

From the figure, it can be seen that the zero-points of the flux calibrations are correct. The experimental

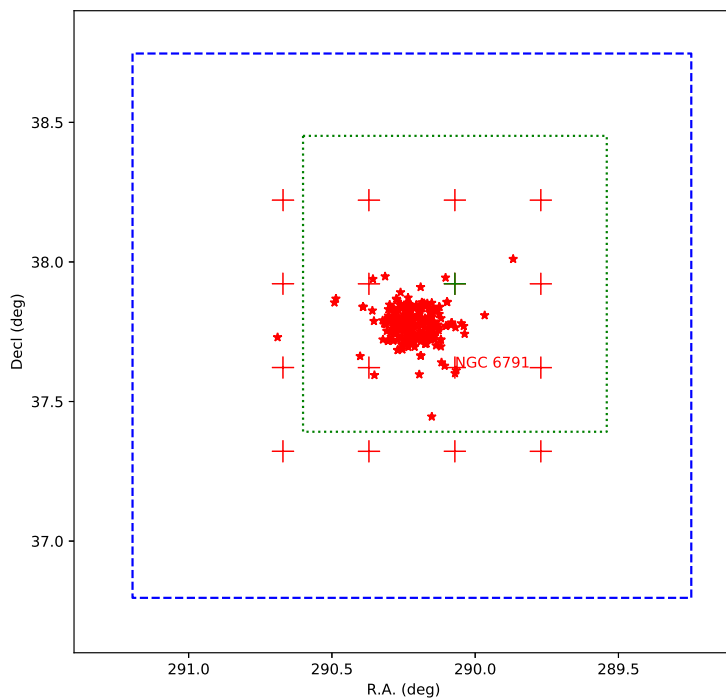


Fig. 12: The footprint of the test observations carried around NGC 6791. The blue dashed box shows the coverage of the test observation, and the 16 crosses are the center of each pointing, while the green dotted box shows the field-of-view of the 90Prime centered at the green cross. The red stars denote the identified members of NGC 6791.

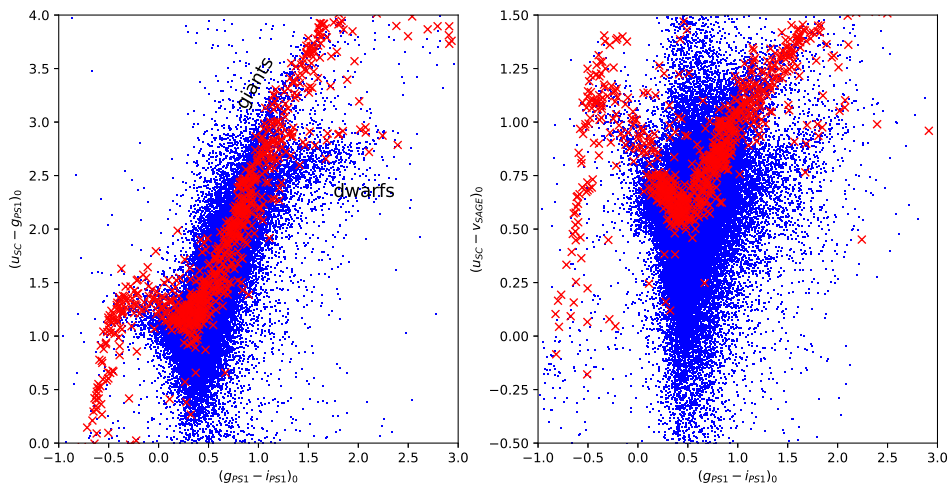


Fig. 13: The dereddened SAGE Colors of stars (blue dots) detected in the test field around NGC 6791, the red crosses are synthetic colors of stars from the MILES stellar library.

5 SUMMARY

The SAGE photometric system is a specifically-designed system including some existing filters and some newly-designed filters. This system is highly sensitive to stellar atmospheric parameters. We have started the SAGE survey since 2015, now about half of the observations is accomplished.

In this work, we describe basic technical details of SAGES including instruments used for observations and pipeline for image process and data analysis. There is still quite some room to improve image reduction, astronomical calibration, and flux calibrations. Around 2020, we expect to obtain high-quality photometry in 8 colors of about 500 million stars, and reliable measurements of their atmosphere parameters, as well as high-spatial resolution and reliable extinction map. We believe that SAGES will produce important observation resource for stellar physics and structure and evolution of the Milky-way Galaxy.

But our data reduction pipeline is not perfect, we are still working on improving it. The stripes in images need to be removed. And the photometric reference catalogue of u_{SC} and v_{SAGE} is also under planning. Meanwhile, we are trying to perform flux evaluation with a higher precious.

Acknowledgements We thank Prof. Micheal Bessell and the SkyMapper team from Research School of Astronomy and Astrophysics, Australian National University (RSAA, ANU) for their help and concern in the SAGE survey. Prof. Richard Green, Prof. Xiaohui Fan, and other astronomers of the Steward Observatory, the University of Arizona, especially the mountain operation team provide great help in observation and data reduction, thanks for them. And we also receive advice from BATC group of NAOC. We appreciate help from all of them. This work is supported by the National Science Foundation of China (11373003, 11673030, & U1631102), National Key Basic Research Program of China (973 Program, 2015CB857002), and National Program on Key Research and Development Project (2016YFA0400804).

References

- Árnadóttir, A. S., Feltzing, S., & Lundström, I. 2010, *A&A*, 521, A40
- Basu, S., Grundahl, F., Stello, D., et al. 2011, *ApJ*, 729, L10
- Bertin E., 2006, *Astronomical Society of the Pacific Conference Series*, 351, 112
- Bertin E. and Armouts S.. 1996, *American Association of Pharmaceutical Scientists*, 117, 393
- Chambers K. C. et al., 2016, arXiv:1612.05560
- Crawford, D. L., Barnes, J. V., & Golson, J. C. 1970, *AJ*, 75, 624
- Ehgamberdiev, S. A., Baijumanov, A. K., Ilyasov, S. P., et al. 2000, *A&AS*, 145, 293
- Falcón-Barroso, J.; Sánchez-Blázquez, P.; Vazdekis, A., et al., 2011, *A&A*, 532A, 95
- Fan Z., Zhao G., Wang W., et al., 2018, *Progress in Astronomy*, accepted
- Freyhammer, L. M., Andersen, M. I., Arentoft, T., et al. 2001, *Experimental Astronomy*, 12, 147
- Fukugita, M., Ichikawa, T., Gunn, J. E., et al. 1996, *AJ*, 111, 1748
- Gaia Collaboration, Brown, A. G. A., Vallenari, A., et al. 2018, arXiv:1804.09365
- Hauck, B., & Mermilliod, M. 1998, *A&AS*, 129, 431
- Hawkins, K., Masseron, T., Jofré, P., et al. 2016, *A&A*, 594, A43
- Howell, S. B. 1989, *PASP*, 101, 616
- Johnson, H. L., & Morgan, W. W. 1953, *ApJ*, 117, 313
- Li, H., Aoki, W., Zhao, G., et al. 2015, *PASJ*, 67, 84
- Li, Y.-B., Luo, A.-L., Zhao, G., et al. 2015, *Research in Astron. Astrophys. (RAA)*, 15, 1364
- Liu, J., Zhang, Y., Feng, G., & Bai, C. 2014, *Setting the scene for Gaia and LAMOST*, *Proc. IAU Symp.*, 298, 427
- Mészáros, S., Holtzman, J., García Pérez, A. E., et al. 2013, *AJ*, 146, 133

- Pickles, A. J. 1998, *PASP*, 110, 863
- Roeser S., Demleitner M., and Schilbach E., 2010, *AJ*, 139(6), 2440
- Roser S., Schilbach E., Schwan H., et al., 2008, *A&A*, 488, 401
- Schlegel, D. J., Finkbeiner, D. P., & Davis, M. 1998, *ApJ*, 500, 525
- Shi, Z. X., Comte, G., Luo, A. L., et al. 2014, *A&A*, 564, A89
- Shupe D. L., Moshir M., Li J., et al., 2005, *Astronomical Society of the Pacific Conference Series*, 347, 491
- Skrutskie, M. F., Cutri, R. M., Stiening, R., et al. 2006, *AJ*, 131, 1163
- Smolinski, J. P., Lee, Y. S., Beers, T. C., et al. 2011, *AJ*, 141, 89
- Strömgren, B. 1963, *QJRAS*, 4, 8
- Strömgren, B. 1964, *Astrophysica Norvegica*, 9, 333
- Tofflemire, B. M., Gosnell, N. M., Mathieu, R. D., & Platais, I. 2014, *AJ*, 148, 61
- Wang, W., Zhao, G., Chen, Y., & Liu, Y. 2014, *Setting the scene for Gaia and LAMOST*, *Proc. IAU Symp.*, 298, 326
- Warren, S. R., & Cole, A. A. 2009, *MNRAS*, 393, 272
- Wolf, C. et al., 2018, *Publications of the Astronomical Society of Australia*, 35, e010
- York, D. G., Adelman, J., Anderson, J. E., Jr., et al. 2000, *AJ*, 120, 1579
- Zhao, G., Zhao, Y.-H., Chu, Y.-Q., Jing, Y.-P., & Deng, L.-C. 2012, *Research in Astron. Astrophys. (RAA)*, 12, 723
- Zhao, J. K., Luo, A. L., Oswalt, T. D., & Zhao, G. 2013, *AJ*, 145, 169
- Zou H., Zhang T.-M., Zhou Z.-M., et al., 2017, *AJ*, 153, 276